Organization of Human Interferon γ−Heparin Complexes from Solution Properties and Hydrodynamics†

Horacio Perez Sanchez,‡,§ Karine Tatarenko,§,|| Michael Nigen,§,|| Georges Pavlov,||,⊥ Anne Imberty,@ Hugues Lortat-Jacob,|| Jose Garcia de la Torre,‡ and Christine Ebel*,||

Departamento de Quimica Fisica, Universidad de Murcia, 30071 Murcia, Spain, Institut de Biologie Structurale, UMR 5075 CEA-CNRS-UJF, 41 rue Jules Horowitz, 38027 Grenoble Cedex 1, France, Institute of Physics, St. Petersburg University, Ulianovskaya Street 1, 198504 St. Petersburg, Russia, and CERMAV-CNRS (Affiliated with Université Joseph Fourier), BP 53, 38041 Grenoble cedex 9, France

Received July 24, 2006; Revised Manuscript Received September 6, 2006

ABSTRACT: Heparan sulfate (HS) recognizes a variety of proteins, one of which is the pleiotropic cytokine IFN-γ, and as such modulates many biological processes. IFN-γ is a homodimer with a well-defined core and two flexible C-termini that constitute HS binding domains. We show here using molecular modeling that an extended IFN-γ structure overlaps a HS fragment of 16 disaccharides (16 nm). Since a 21−24-disaccharide HS fragment was experimentally defined as the minimum size that interacts with IFN-γ [Lortat-Jacob, H., Turnbull, J. E., and Grimaud, J. A. (1995) *Biochem. J. 310* (Part 2), 497−505], this raises the question of the complexe organization. We combine analytical ultracentrifugation, size exclusion chromatography, and hydrodynamic bead modeling to characterize the complexes formed in solution with heparin oligosaccharides. For oligosaccharides of 14 and 20 nm, two types of complexes are formed with one IFN-γ and one or two heparin molecules. Complexes consisting of two IFN-γ and one or two heparin molecules are present for a fragment of 25 nm and aggregates for a fragment of 35 nm. The complexes are rather compact and can be formed without major conformational changes of the partners. The complex pattern of interaction is related to the size of the partners and their multiple binding possibilities. These various possibilities suggest networks of interactions at the crowded surface of the cells. Hydrodynamic methods used here proved to be very efficient tools for describing protein−HS complexes that, due to the intrinsic heterogeneity and flexibility of the partners, are otherwise very difficult to analyze.

Heparan sulfates (HS)[1] are found in the extracellular matrix of organisms and at the cell's surface, where they are linked to various proteins to form proteoglycans (*1*, *2*). HS are essential in various fundamental biological processes, in particular those related to the communication of the cell with or the response to the environment. For example, they are involved in growth control, regulation of cell adhesion and morphology, inflammatory reaction, and lipid metabolism. They can be used also by pathogens as attachment or entry receptors or to promote or inhibit tumor growth and metastasis (*3*−*5*). At the cellular level, their effects are related to their interaction with a large variety of proteins. HS allows the localization of proteins in tissues and their protection against proteolysis and favors their multimerization and their association with membrane receptors, i.e., modulates their activities. The study of the interactions of HS with their proteic partners is thus the object of strong interest.

HS are linear polysaccharides that belong to the glycosaminoglycan family. Like heparin, they are based on alternating 1→4-linked residues of hexuronic acid and D-glucosamine (GlcN), the sugars being heterogeneously substituted. Hexuronic acid is either β-D-glucuronic acid (GlcA) or its C5 epimer α-L-iduronic acid (IdoA) and can be O-sulfated at the C2 position. GlcN can be N-acetylated or N-sulfated and O-sulfated at the C6 and C3 positions. HS possesses alternate domains of weakly (called A-domains) and highly negatively charged (heparin-like or S-domains) domains, between which mixed A/S-regions make the transition (*6*−*8*). Due to the extreme chemical and conformational heterogeneity of HS or heparin fragments, the high-resolution structures of the related complexes are obtained with difficulty. High-resolution structures show only polysaccharides of limited size in contact with the proteins (see ref *9* for a review and http://www.cermav.cnrs.fr/glyco3d/index.php for database complexes of three-dimen-

† This work was supported by the CNRS, the CEA, and the University Joseph Fourier (Grenoble, France). G.P. and H.P.S. were recipients of fellowships from the CEA and European Community Marie-Curie Short Training Grant HPMT-CT-2001-00342.

* To whom correspondence should be addressed. Telephone: (33)(0)4 38 78 96 38. Fax: (33)(0)4 38 78 54 94. E-mail: christine.ebel@ibs.fr.

‡ Universidad de Murcia.

§ These authors have contributed equally to this work.

|| Institut de Biologie Structurale CEA-CNRS-UJF.

⊥ St. Petersburg University.

@ CERMAV-CNRS (Affiliated with Université Joseph Fourier).

[1] Abbreviations: A-domains, N-acetylated glucosamine rich (weakly charged) domains of heparan sulfate; AUC, analytical ultracentrifugation; GlcA, β-D-glucuronic acid; GlcN, D-glucosamine; $Hep_{19.9}$, $Hep_{14.1}$, $Hep_{11.2}$, and $Hep_{7.7}$, fractions of heparin with molecular masses of 19.9, 14.1, 11.2, and 7.7 kDa, respectively; HS, heparan sulfate(s); IdoA, α-L-iduronic acid; IFN-γ, interferon γ; MC, Monte Carlo; S-domains, N-sulfated glucosamine rich (highly negatively charged) domains of heparan sulfate; SEC, size exclusion chromatography; SV, sedimentation velocity.

10.1021/bi061490w CCC: $33.50
Published on Web 10/17/2006

sional structures). Different complexes with growth factors, which are biologically similar, have been obtained with different geometries and stoichiometries (*10*). It is thus possible that chemical contacts are established in relation to the crystalline state. Molecular modeling approaches have been used for protein−HS complexes (*11*). They demonstrate the possibility of very different geometries of association for complexes of HS with chemokines. These unexpected differences in association states and topology, in addition to the intrinsic difficulty in gathering high-resolution information, motivate complementary structural approaches to characterization of HS−protein complexes in solution, a point that we analyzed here with interferon γ (IFN-γ).

IFN-γ is a pleiotropic cytokine with antiviral, antiproliferative, and immunostimulating properties (*12*, *13*). Secreted by T-lymphocytes and natural killer cells, it interacts with a specific membrane receptor expressed on the surface of all cells. As a consequence, a complex cascade of events leads to gene transcription of a variety of proteins (*7*, *14*, *15*). In addition to its cell surface receptor, IFN-γ also binds to HS with high affinity ($K_d = 1.5 \times 10^{-9}$ M) (*16*). In vivo studies showed that binding of IFN-γ to HS controls the blood clearance, the subsequent tissue targeting, and the local accumulation of the cytokine (*17*, *18*). These observations suggest a mechanism by which IFN-γ is rapidly captured by HS in the vicinity of the secreting cells, thus ensuring a localized action of the cytokine. This interaction was also shown in vitro to protect the cytokine from proteolysis (*19*). The protein is active as a homodimer, each polypeptide chain having 143 amino acids (33 552 Da). The crystallographic structure of bovine and human proteins either unliganded or bound to the receptor ectodomain shows each monomer organized with six α-helices linked by loops (*20*−*23*). However, the resolution is 2 Å only for rabbit, and none of these structures revealed the organization of the last 20 amino acids at each C-terminus which were thus believed to be unstructured or highly flexible. They contain two small clusters of basic amino acids [C1, residues 125−131 (KTGKRKR); C2, residues 137−140 (RGRR)] which constitute the HS binding domain (*24*), confer to the molecule the sensitivity to a variety of proteases, and modulate binding to the receptor (*25*).

On Figure 1, we have juxtaposed the NMR structure of a heparin fragment comprising six disaccharides (*26*) (PDB entry 1HPN) with that of human IFN-γ obtained by crystallography (*20*) (PDB entry 1HIG). Only the first 123 amino acids of IFN-γ are presented in this figure; the distance between the two C-termini is only 2 nm. However, using a footprinting approach, in which fibroblast-derived HS was depolymerized in the presence of IFN-γ, a protected domain was isolated which consists of an extended internal domain (15−16 disaccharides) predominantly N-acetylated and GlcA-rich, flanked by small N-sulfated oligosaccharides (mainly hexa- to octasaccharides), for a total of 21−24 disaccharides (*27*). A rigid fragment of 24 disaccharides, 4 times larger than that presented in Figure 1, would have a total length of 21 nm, which corresponds to the experimental value of 25 nm determined for heparin that is similar in size (*28*). Such a large size for HS interacting with IFN-γ suggests a very extended configuration of the protein on HS, on which the two external S-regions are believed to interact with the two carboxy-terminal sequences of an IFN-γ dimer and bridge the two IFN-γ monomers by virtue of the internal A-domain (*27*).

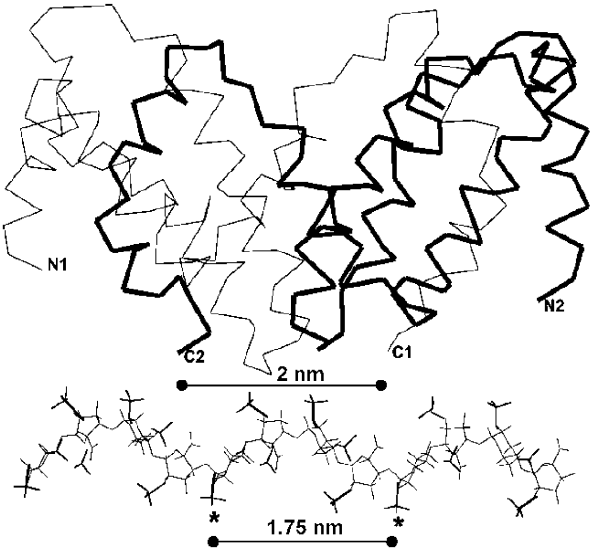

FIGURE 1: IFN-γ core and heparin fragment. The crystallographic structure of the IFN-γ core is from ref *20* (PDB entry 1HIG). The NMR structure of the six-disaccharide heparin fragment is from ref *26* (PDB entry 1HPN). The sulfate groups are depicted in bold. The lines show for IFN-γ the distance between the two visible C-terminal ends (20 residues are not seen in the structure) and the separation between two successive disaccharides. The representation is at the same scale for the two molecules.

The difference in the size of the partners raises the following questions: the minimal size of the HS partner, the possibility of a very elongated structure of IFN-γ in the complex, and possible changes in the structure of the partners. Using a set of glycoconjugates, composed of N-sulfated oligosaccharides linked to each other through different spacers that mimic the IFN-γ binding domain in HS, we recently reported that the optimum ligand was made of two authentic N-sulfated octasaccharides, spaced by a 5 nm long linker, thus having a total size of 11.5 nm (*29*).

We present here the characterization of IFN-γ−heparin species resulting from their interactions in solution. We have used complementary experimental approaches, analytical ultracentrifugation, and size exclusion chromatography, combined with molecular and hydrodynamic modeling, to investigate the numbers of complexes formed in solution, their stoichiometries, and dimensions. We have chosen to use heparin as a model of the highly charged fragments of HS interacting with IFN-γ. The fragments of heparin (between 13 and 34 disaccharides, i.e., 14 and 35 nm) were previously characterized in view of their hydrodynamic properties (*28*).

MATERIALS AND METHODS

Materials

Heparin Samples. The fractionation of heparin sodium salt from porcine intestinal mucosa from Sigma (reference H3393) and characterization of the fragments were previously described (*28*). Four fractions of heparin of different sizes with molecular masses of 19.9, 14.1, 11.2, and 7.7 kDa named $Hep_{19.9}$, $Hep_{14.1}$, $Hep_{11.2}$, and $Hep_{7.7}$, respectively, were chosen for the study of IFN-γ−heparin interactions. Their characteristics are presented in Table 1.

Table 1: Characteristics of Heparin Fractions and IFN-γ[a]

	M ($\times 10^{-3}$ g/mol)	N_{disach}	L (nm)	$s_{20,w}$ (S)	R_h (nm)	M_b ($\times 10^{-3}$ g/mol)	R_h from simulation (MC) (nm)
$Hep_{7.7}$	7.7	13	14	1.7	2.1	4.1	2.2
$Hep_{11.2}$	11.2	19	20	2.0	2.6	5.9	2.7
$Hep_{14.1}$	14.1	24	25	2.2	3.0	7.4	3.1
$Hep_{19.6}$	19.6	34	35	2.5	3.6	10.4	3.9
IFN-γ, dimer	33.6			2.7	3.0	8.6	

[a] M is the molar mass, N_{disach} the number of disaccharides, L the contour length, $s_{20,w}$ the sedimentation coefficient, R_h the hydrodynamic radius, and M_b the buoyant molar mass, calculated from the composition. The characteristics of heparin fragments are from ref *28*, except the data in the last column, which are from this work.

Interferon γ. Human IFN-γ was overexpressed in *Escherichia coli* as inclusion bodies, renatured, and purified essentially as described previously (*30*). All protein solutions contained 1 mM antiprotease (AEBSF hydrochloride, Acros Organics). IFN-γ antiviral activity was determined in triplicate with a standard microtiter inhibition-of-cytopathic-effect assay against VSV on monolayers of WISH cells, essentially as described by Berg et al. (*31*). The specific antiviral activity of freshly purified or lyophilized IFN-γ is 6 units/ng and decreases to 2 units/ng for IFN-γ that was conserved at −20 °C in solution. We observed for a sample of IFN-γ that was conserved at −20 °C in solution a tendency to form larges aggregates in the presence of $Hep_{7.7}$ in solution, from the loss of absorbency of the solution just after it reached 42 000 rpm in the analytical ultracentrifuge. This suggests an alteration of the three-dimensional structure of IFN-γ. Other experiments used freshly prepared IFN-γ, the last step being gel filtration.

Molecular Modeling

Since the only available crystal structure of human IFN-γ has been determined at low resolution with only Cα atoms deposited in the protein database, the structure of dimeric bovine IFN-γ (entry 1RFB) was used as a starting model (*21*). Sybyl (Tripos Inc., St. Louis, MO) was used for appropriate mutations of individual amino acids. The C-terminal sequence (residues 120−143) was built as an extended β-strand and attached to Glu119 on both monomers, resulting in an antiparallel orientation of the two C-terminally added regions. Hydrogen atoms were added, and charges were calculated with the Pullman procedure. The Tripos force field (*32*) was used for optimization of hydrogen atoms position. The geometry of the model was optimized to release any steric constraint while keeping the backbone of amino acids 1−119 fixed.

A heparin fragment consisting of 16 disaccharide repeats was built in the ribbonlike conformation observed in the NMR study (*26*). To mimic the block regions generally observed in heparan sulfate, the 10 internal disaccharides were not (or almost not) sulfated and contain glucuronic acid, whereas the three disaccharides on both sides were highly sulfated and the GlcA residues epimerized in IdoA in a $^1C_4$ conformation. Atom type and charges were selected according to the PIM force field developed for protein−carbohydrate interactions (*33*). Optimization of the complex between IFN-γ and the heparan sulfate fragment was performed with the PIM force field. Accessible surface calculations and drawing were performed with MOLCAD (*34*).

Hydrodynamic Measurements

Sedimentation Velocity. The hydrodynamic experiments were performed with heparin fractions, freshly prepared IFN-γ, or mixtures typically in 10 mM Tris, 35 mM mannitol, and 0.2 M NaCl (pH 6.8). Sedimentation velocity experiments were performed in a Beckman XLI ultracentrifuge at a rotor speed of 42 000 rpm and at 10 °C in double-sector cells with an optical path of 12 mm using absorbency at 280 nm and interference optics. Analysis of the data was carried out according to the $c(s)$ analysis method, using Sedfit (*35, 36*) (available free at www.analyticalultracentrifugation.com). The $c(s)$ method deconvolutes the effects of diffusion broadening, yielding high-resolution sedimentation coefficient distributions. This is done by assuming a plausible relationship between sedimentation and diffusion coefficients, s and D, respectively. The fact that an inadequate relationship between s and D only decreases the details and resolution of the distribution but does not affect the values of s must be mentioned. The $s-D$ relation is based on the values of the particle partial specific volume ($\bar{\nu}$), frictional ratio (f/f°), solvent density (ρ_0), and viscosity (η_0). The solvent viscosity of 0.0143 p and the density of 1.01047 g/mL, at 10 °C, and the $\bar{\nu}$ value of 0.735 mL/g for IFN-γ were calculated using Sednterp (available free at http://www.jphilo.mailway.com/). We considered a $\bar{\nu}$ of 0.467 mL/g for heparin fractions (*28*), and for the complexes, $\bar{\nu} = 0.6$ mL/g, a value intermediate between those for the protein and heparin. We typically used f/f° values of 1.25. Depending on the data, a regularization procedure was applied, which leads to a more regular distribution, or was not. The $c(s)$ distributions were used to derive the corrected sedimentation coefficients $s_{20,w}$ (at 20 °C, in water). From the area under the peaks, we determined the number of fringes (J) and the absorbance signal (A_{280}) corresponding to the different species. To derive the concentration from A_{280}, we consider the molar extinction coefficient (ϵ_{280}) of 22 290 cm^{-1} M^{-1} for IFN-γ from the sequence and an ϵ_{280} of 0 cm^{-1} M^{-1} for heparin. $J = cl(K/\lambda)(\Delta n/\Delta c)$, with values for the refractive index increment ($\Delta n/\Delta c$) being 0.188 mL/g for IFN-γ, a typical value for protein, and 0.132 mL/g for heparin (*28*), where c is the concentration here expressed in grams per milliliter, l is the path length in centimeters, and the K/λ for our device is 6.85 $\times$ 10^{-5} cm. The value of the sedimentation coefficient s is related with molecular characteristics by the Svedberg relationship:

$$s = M(1 - \bar{\nu}\rho_0)/(N_A 6\pi\eta_0 R_h) = M_b/(N_A 6\pi\eta_0 R_h) \quad (1)$$

where M is the molar mass, $1 - \bar{\nu}\rho_0$ is the buoyancy factor, M_b is the buoyant molar mass, N_A is Avogadro's number, and R_h is the hydrodynamic radius of the macromolecule. As a consequence, the s value is related to the ratio M_b/R_h.

Size Exclusion Chromatography. Calibrated size exclusion chromatography was performed to determine the hydrodynamic radius of the macromolecular species in solution. The solution (250 μL) was injected on a Superose-12 HR10-30 column (Pharmacia Biotech) in a cold room, at a flow rate of 0.5 mL/min, and elution profiles were recorded at 280 nm. A calibration equation was obtained by a linear fit of

the partition coefficient as a function of $\log(R_h)$, using the Amersham Pharmacia Biotech kit of eight proteins with known R_h values, between 1.64 nm (ribonuclease A) and 8.5 nm (thyroglobulin), and used to estimate the hydrodynamic radius of IFN-γ complexes.

Complex Stoichiometry from Sedimentation Velocity and Size Exclusion Chromatography. Using eq 1, the buoyant molar mass is obtained from s and R_h. These values can be compared with calculated values for different stoichiometries. For a complex composed of n_i subunits of type i, each characterized by a molar mass M_i and partial specific volume $\bar{\nu}_i$:

$$M_b = \sum n_i M_i (1 - \bar{\nu}_i \rho_0) \quad (2)$$

Hydrodynamic Modeling

General Principle of Hydrodynamic Modeling. HYDRO (*37*) is used to calculate the hydrodynamic properties for macromolecules defined as assemblies of nonoverlapping beads of different or equal hydrodynamic radii. The program provides general hydrodynamic properties from which are derived the translational diffusion coefficient (D_t) related to R_h by $D_t = (kT)/(6\pi\eta_0 R_h)$, where k is Boltzmann's constant and T the absolute temperature (*7*), as well as geometrical quantities such as the radius of gyration (R_g).

Different strategies were used, with the help of several computer simulation techniques, to define the bead assemblies for the partners and complexes. In the rigid cases, the solution properties of the macromolecule calculated with HYDRO are compared with experimental values, to accept or reject the model of bead assemblies following certain acceptance criteria. In the flexible cases, the statistical properties are calculated following Monte Carlo (MC) or Brownian dynamics simulations. The heparin fragments were modeled first as a wormlike chain composed of beads and characterized by its constant flexibility and diameter of beads but variable contour length (*38*, *39*). Rigid assemblies of beads, where Cartesian coordinates and hydrodynamic radii are specified for each bead, were considered in the modeling of IFN-γ and the complexes.

Parameters Used for Heparin. Using an appropriate notation (*40*) and considering the experimental results obtained for the heparin fragments used in the work presented here (*28*), the following values are assumed for a wormlike cylinder model: persistence length P of 5.0 nm, linear mass density M_L of 570 Da/nm, and cylinder diameter d of 1.0 nm. The wormlike chain bead model for heparin is a semiflexible chain of N beads with diameter b (radius $a = b/2$). The diameter of the beads is selected so that the volume of the string of beads is the same as the volume of the "hydrodynamic cylinder". This gives a d of $0.8165b$. For heparin, $b = 1.22$ nm and $a = 0.61$ nm. The contour length L must be the same as that calculated from M and M_L, i.e., $L = M/M_L = Nb$. Then we have $N = 0.8165M/(dM_L)$. The derived numbers of beads, N, are 28 for $Hep_{19.9}$, 20 for $Hep_{14.1}$, 16 for $Hep_{11.2}$, and 11 for $Hep_{7.7}$. The bending constant (Q) is determined using the relationship $Q = P/b$ (*38*).

Monte Carlo Simulation. Equilibrium properties of the heparin fragments are calculated with a wormlike model (*38*, *39*) in a homemade computer program where the Metropolis algorithm (*47*) is implemented. An ensemble of molecules (typically around 100 000) in equilibrium is generated when this simulation technique is applied individually to initially random configurations of molecules. After a finite number of simulation steps (typically around 10 000), average values and standard deviations for the hydrodynamic properties are calculated with HYDRO over the sample.

Brownian Dynamics. A Brownian dynamics simulation technique implemented with a homemade computer program called BROWFLEX developed by García de la Torre et al. (*40*) was applied to the wormlike models for the heparin fragments to obtain the equilibrium properties. For five different molecules of each of the heparin fragments, and using a wormlike model, a Brownian trajectory was simulated with time steps of 0.43 ps for a total of 8.6 μs, leading to equilibrium conditions. Average values over time for the hydrodynamic properties were obtained in each trajectory. Global average values and standard deviations were obtained for the hydrodynamic properties. The diffusion coefficient can be calculated following two different procedures: from equilibrium properties and from translational correlation functions. In this last case, hydrodynamic interaction between the beads of the model has been taken into account in calculations using a second-order algorithm (*41*).

Parameters Used for IFN-γ. Taking into account the globular shape observed for interferon γ by X-ray crystallography [PDB entry 1hig (*20*)] and the missing flexible ends that are not seen in the crystals as protuberances, we used a bead with hydrodynamic radius a_1 to represent the core of the protein and a linear rigid chain of N_s beads with hydrodynamic radius a_2 (considering $a_1 > a_2$) to represent the protuberances (Figure 6). Models for the protein are accepted or discarded using a computer program that compares the calculated hydrodynamic radius, with HYDRO, to the experimental one. It makes a loop over a large number of different combinations of values for a_1, a_2, and N_s.

Parameters Used for the Complexes. We considered the simple models in which each of the partners consists of a rigid bead assembly and its structure does not change upon association, except for the arms of IFN-γ. For IFN-γ, we used one of the models defined above. For heparin, we considered a rigid assembly of beads composed of successive linear segments, with the number and dimension of beads considered in the wormlike model, the length of the segment minus four beads, of 4.9 nm, which is close the value of the persistence length, and the angle between the segment of 140.5° being chosen to reflect the ratio of the contour length and mean end-to-end distance of the segments. Sedimentation coefficients were calculated with HYDRO, with the molar masses and partial specific volumes from complex stoichiometries for comparison with the experimental values.

RESULTS

Hydrodynamic methods were used to analyze the association process. Analytical ultracentrifugation (AUC) was found to be powerful in revealing different associated states in addition to the IFN-γ and heparin fragments remaining free in solution. The experiments were performed using two optical systems, absorbance and interference, the former revealing the presence of the protein and the latter being

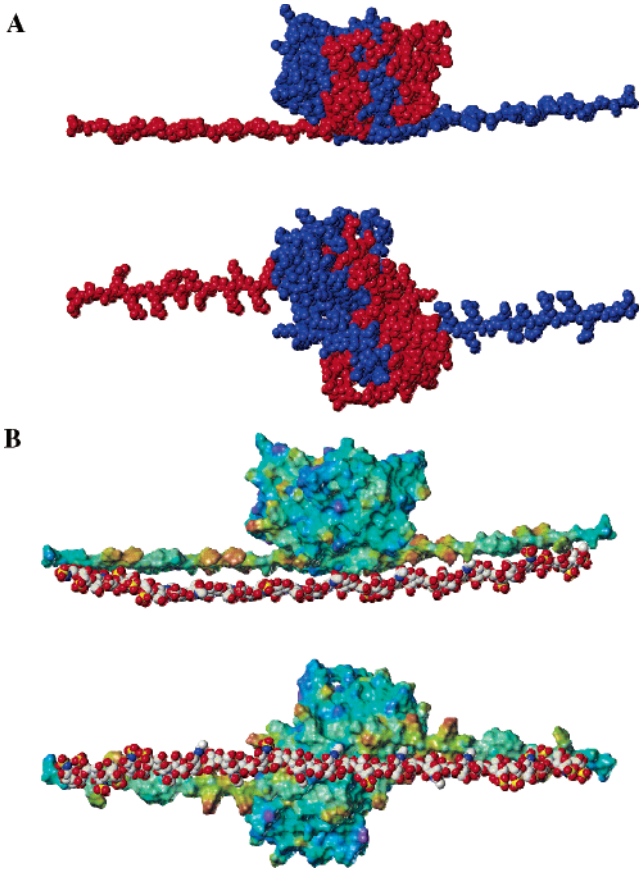

FIGURE 2: Molecular modeling of IFN-γ with fully extended C-terminal regions. (A) Two perpendicular views of the dimer (space-filling representation with hydrogen atoms not shown) with the two monomers colored red and blue. (B) Two perpendicular views of the complex with the heparan sulfate displayed as a space-filling model and the protein represented by its Connolly surface color-coded according to the electrostatic potential (from blue for the negatively charged area to red for the positively charged area).

related to the protein and heparin component. Size exclusion chromatography (SEC), which is also a separative and analytical method, provides a complementary description of the association process. The hydrodynamics characteristics from the two methods, the sedimentation coefficients and hydrodynamics radii, were combined in proposing a composition for the different complexes. The optical properties of the complex were used to propose a composition for the complexes. Hydrodynamic modeling together with molecular modeling was used to check if the proposed association states were compatible with the hydrodynamic properties of the complexes.

Molecular Modeling of an Extended Form of Whole IFN-γ

The model of the complex of human IFN-γ with a fully extended C-terminal region is represented in Figure 2A. In such a model, where the region of residues 120−143 adopts a β-strand conformation, the distance between the two C-terminal extremities of the dimer is more than 160 Å. This corresponds to the size of a heparan sulfate fragment of 16 disaccharides. The proposed complex between IFN-γ and heparan sulfate is displayed in Figure 2B. The clusters of basic amino acids located at the C-termini of both monomers are involved in the binding of heparan sulfate, whereas the central region does not participate much in the interaction.

Sedimentation Velocity and Size Exclusion Chromatography Experiments Indicate Different Types of Complexes

Sedimentation velocity AUC experiments with IFN-γ at 20 μM incubated with the largest fraction of heparin ($Hep_{19.6}$, 19 600 g/mol, 34 disaccharides) at three concentrations (20, 10, and 5 μM) revealed aggregation, since the first sedimentation profiles showed no absorbencies at 280 nm, i.e., no protein. Heparin of this size is possibly too large for the formation of soluble complexes with IFN-γ. In contrast, the right panels in Figure 3 show a well-defined complex, detected at an $s_{20,w}$ of 4.5 S in absorbance and by interference, for a sample of IFN-γ at 13 μM incubated with 60 μM $Hep_{14.1}$ (14 100 g/mol, 24 disaccharides). In addition to the complex, unbound $Hep_{14.1}$ is detected by interference at an $s_{20,w}$ of 2.1 S, a value that almost coincides (with an accuracy of 0.1 S) with published values (*28*). Figure 3 shows for comparison the profiles obtained under the same conditions and the analysis for IFN-γ ($s_{20,w}$ = 2.7 S) (left panels) and heparin fragments separately (panels at the center).

The same AUC procedure was used for different mixtures. In the case of IFN-γ in the presence of $Hep_{14.1}$, depending of the concentrations of the constituents, one or two types of complex were discerned. For example, with IFN-γ at 20 μM and $Hep_{14.1}$ at 28 μM, a larger complex at an $s_{20,w}$ of 6.1 S in addition to the complex at an $s_{20,w}$ of 4.5 S is well represented: its absorbance is half that of the 4.5 S one (data not shown). In the presence of the shorter fragments of heparin, $Hep_{11.2}$ (11 200 g/mol, 19 disaccharides) and $Hep_{7.7}$ (7700 g/mol, 13 disaccharides), two types of complex were again detected. They were found in similar amounts for IFN-γ and heparin fragments in the 10 μM range. For the IFN-γ/$Hep_{7.7}$ series, the concentration dependency of the proportion of the two types of complexes is clearly seen in Figure 4, with an increasing proportion of the larger species with an increase in $Hep_{7.7}$ concentration.

Size exclusion chromatography separates the species according to their sizes. Some of the samples characterized by SV experiments were analyzed with SEC. In the case of complexes of IFN-γ with $Hep_{14.1}$ and $Hep_{11.2}$, the two complexes were unresolved (not shown). In the case of IFN-γ/$Hep_{7.7}$ mixtures, two peaks are distinguished, with the proportion of the larger species increasing at the larger concentration of $Hep_{7.7}$, in agreement with AUC observations (Figure 4). The hydrodynamic radii obtained from calibration with proteins of known R_h are given in Table 2. The complexes are larger than the partners (see Table 1), except for the smaller complex, from the interaction of IFN-γ and $Hep_{7.7}$, which has the same R_h as IFN-γ.

Combining AUC and SEC in Determining the Composition of the Complexes

From the combination of the sedimentation coefficients from AUC and hydrodynamic radii from SEC, the buoyant molar masses (M_b) were calculated. They are given in Table 2. The M_b values of complexes are significantly larger that the M_b values of initial components (Table 1), a net proof of formation of a complex between IFN-γ and heparin molecules.

Complexes of IFN-γ and $Hep_{7.7}$. The two complexes have buoyant molar masses that fit with complexes associating

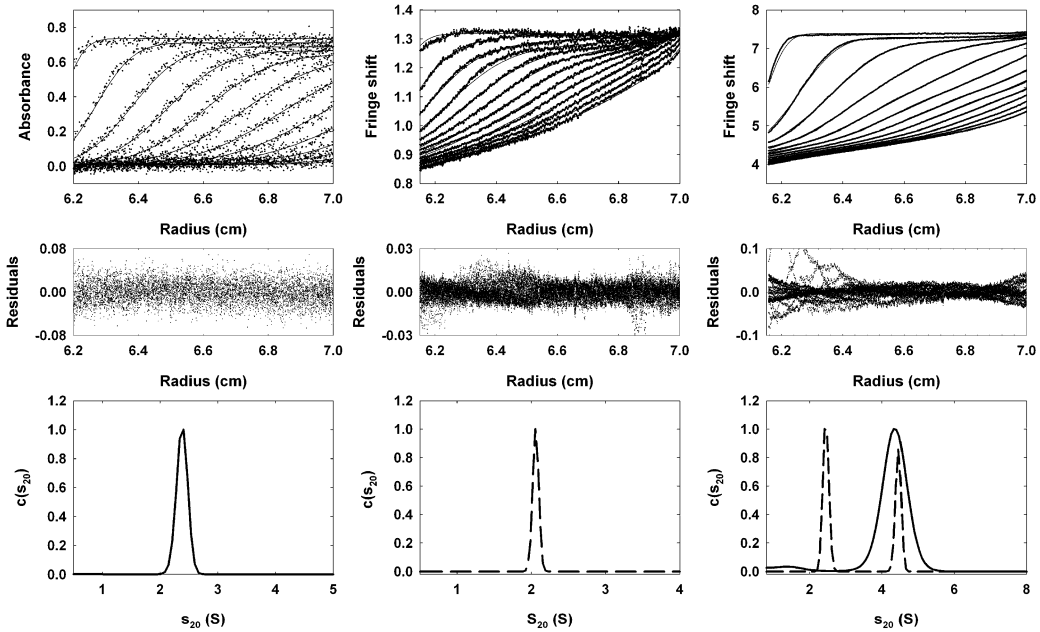

FIGURE 3: Sedimentation profiles of 18 μM IFN-γ (left), 10 μM Hep$_{14.1}$ (center), and the mixture of 13 μM IFN-γ and 60 μM Hep$_{14.1}$ (right). Panels at the top show the superposition of 13 profiles obtained with absorbance at 280 nm (left) and interference optics (center and right) for 770 min at 10 °C and 42 000 rpm. Panels at the middle show the corresponding residual plots. Panels at the bottom represent the distribution of sedimentation coefficients corrected at 20 °C, obtained by absorbance (—) and/or interference (− − −). The distributions were obtained with a regularization procedure with a confidence level of 0.68 and are normalized for a maximum value of 1.

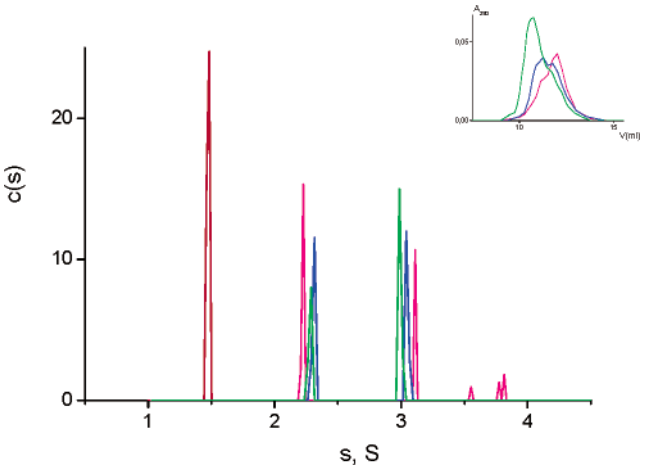

FIGURE 4: Sedimentation velocity of IFN-γ/Hep$_{7.7}$ mixtures at 10 °C. Distributions of sedimentation coefficients [$c(s)$] were obtained without a regularization procedure for 18 μM Hep$_{7.7}$ using interference optics (red), mixtures of 18 μM IFN-γ and 9 (pink), 18 (blue), or 36 μM Hep$_{7.7}$ (green) using A_{280}. Using interference optics, three peaks at approximately the same s values are detected for the mixtures (not shown). Sedimentation coefficients are experimental, and corrected $s_{20,w}$ values are reported in Table 2. The inset shows the shape of the elution peak from size exclusion chromatography with the same color codes.

one molecule of IFN-γ with one or two molecules of heparin. The fact that the larger complex has an increased heparin content when compared to the smallest one is in agreement with the observations made by AUC and SEC: its proportion increases when compared to the 1:1 complex with an increase in heparin concentration.

Complexes of IFN-γ and Hep$_{11.2}$. The two species have different s values but were not distinguished by SEC. The smallest complex has an estimated M_b of 17 kDa from s and R_h, which is compatible with a 1:1 or 1:2 IFN-γ/Hep$_{11.2}$ stoichiometry. The M_b value of 23 kDa for the largest complex would correspond to a 1:2 or 2:1 stoichiometry, when considering the R_h value of the unique peak observed by SEC. To resolve the ambiguity, and also considering that the R_h value for the large complex can be uncertain, we exploited the information given by the areas under the peaks of the $c(s)$ profiles. Absorbance is related to IFN-γ concentration and interference to the IFN-γ and Hep$_{11.2}$ ones. Even if the concentrations determined for Hep$_{11.2}$ are not very precise, this protocol leads to an estimate, for the smallest species at 3.6 S, of a content of 6 μM IFN-γ and Hep$_{11.2}$, which coincides perfectly with the 1:1 complex. For the largest species at 4.9 S, a content of 4 μM IFN-γ and 10 μM Hep$_{11.2}$ is estimated and is compatible with the 1:2 IFN-γ:Hep$_{11.2}$ stoichiometry proposed considering the value of M_b.

Complexes of IFN-γ and Hep$_{14.1}$. One or two complexes are detected from AUC. The main and smaller one has an M_b value of 27 kDa, which is compatible with different stoichiometries of 2:1, 1:2, and 2:2. From the integration of the $c(s)$ peak presented in Figure 3, corresponding to loading concentrations of 13 μM IFN-γ and 60 μM Hep$_{14.1}$, the complex would comprise 12 μM IFN-γ and 7 μM Hep$_{14.1}$. For a sample composed of 20 μM IFN-γ and 28 μM Hep$_{14.1}$ (data not shown), the main smallest complex would also comprise an excess of IFN-γ when compared to Hep$_{14.1}$ (rough estimates of 16 and 3 μM), while the largest ones have nearly the same molar amounts of the partners (rough estimates of 7 μM IFN-γ and 9 μM Hep$_{14.1}$). This suggests that the smallest complex comprises two IFN-γ molecules bound to one molecule of Hep$_{14.1}$. For the largest species, the buoyant molar mass of 37 kDa derived from s and R_h experiments and the estimates of concentrations from the $c(s)$ profiles suggest, more speculatively but reasonably, that the largest would comprise two IFN-γ molecules bound to two Hep$_{14.1}$ molecules.

Table 2: Characteristics of Complexes of Heparin with IFN-γ[a]

		$s_{20,w}$ (S)	R_h (nm)	M_b ($\times 10^{-3}$ g/mol) ± 10%	from AUC	theoretical M_b ($\times 10^{-3}$ g/mol) 1:1[b]	1:2[b]	2:1[b]	2:2[b]	proposed
IFN-γ−Hep$_{7.7}$ ($N_{disacch}$ = 13)	complex 1	3.4 ± 0.1	3.0	11.2	nd[c]	**12.7**	*16.8*	*21.3*	*25.4*	1:1
	complex 2	4.4 ± 0.1	3.8	18.5	nd[c]	12.7	**16.8**	*21.3*	*25.4*	1:2
IFN-γ−Hep$_{11.2}$ ($N_{disacch}$ = 19)	complex 1	3.6 ± 0.3	4.2	16.8	1:1	**14.5**	*20.4*	*23.1*	*29*	1:1
	complex 2	4.9 ± 0.3	4.2	22.8	1:2.5	*14.5*	**20.4**	*23.1*	*29*	1:2
IFN-γ−Hep$_{14.1}$ ($N_{disacch}$ = 24)	complex 1	4.5 ± 0.2	5.4	27.0	1:0.4	*16.0*	*23.4*	**24.6**	*32*	2:1
	complex 2	6.1 ± 0.2	5.4	37.0	1:1.3	*16.0*	*23.4*	*24.6*	**32**	2:2

[a] The buoyant molar masses (M_b) were obtained from the measured values of $s_{20,w}$ and R_h. The compositions from AUC are determined from the intensities of signals obtained by interference and absorbance in the $c(s)$ analysis of sedimentation velocity. These ratios and the theoretical values of M_b were used to infer the composition of the different complexes. In bold are the theoretical values of M_b corresponding to the association states of the complexes evidenced in solution. See the details in the text. [b] IFN-γ:heparin fragment composition. [c] Not determined (this set of experiments let to imprecise values).

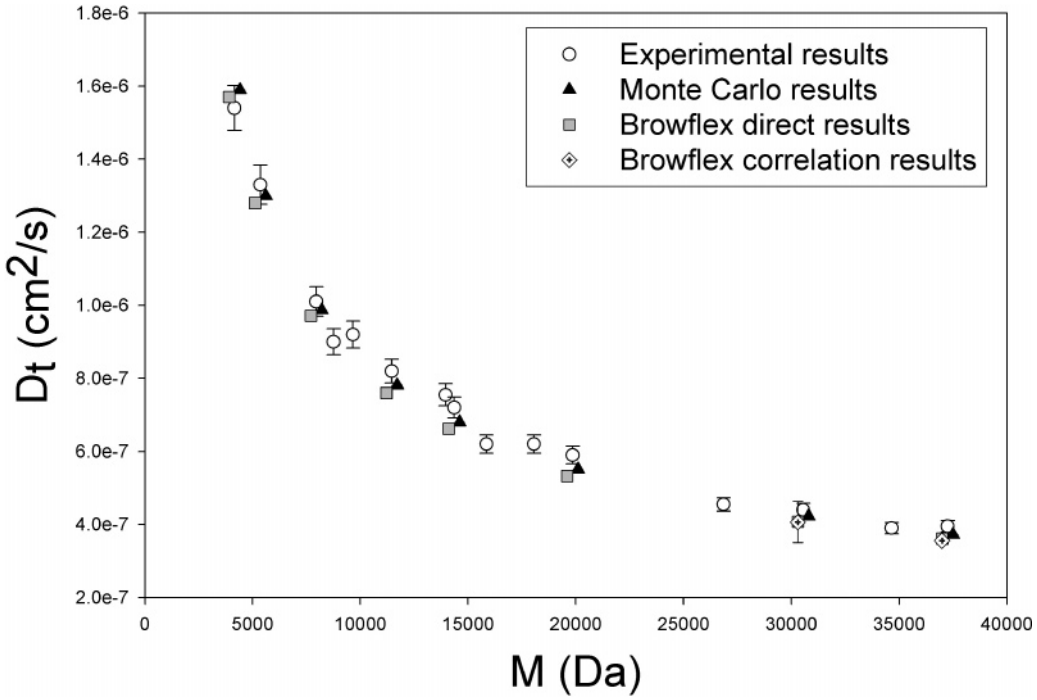

FIGURE 5: Translational diffusion coefficients (D_t) of heparin fragments. Comparison between experimental (*28*) and simulation results for the hydrodynamic modeling of the heparin fragments. Results are shifted in M to appreciate error bars.

Table 2 summarizes the characteristics of the complexes and their proposed stoichiometries. There is not an obvious correlation between those and the values of the sedimentation coefficients, hydrodynamics radii, and buoyant molar masses. This motivates the hydrodynamic modeling study presented here.

Hydrodynamic Modeling

Hydrodynamic Modeling of Heparin. Three different simulation methods have been used to calculate steady state properties for hydrodynamic wormlike models of heparin. The Monte Carlo simulation method has been implemented in a homemade computer program. Browflex has been used to run long Brownian dynamics trajectories for the bead model; Browflex has also been used to run trajectories with hydrodynamic interaction for obtaining the correlation function for translational diffusion. Calculated properties have been compared with Pavlov's experimental results (*28*). A very good agreement is found for R (end-to-end distance), R_g (radius of gyration), D_t (diffusion coefficient), and, for most of the fragments, [η] (intrinsic viscosity). [η] is known to be much sensitive to the details of the modeling. The values for [η] obtained from Browflex are scattered for the two longer fragments above 30 000 g/mol, with differences with experimental values of up to 40%, in probable relation to the limited trajectories (data not shown). Figure 5 shows the results for D_t. On Table 1, we have reported the related R_h values obtained from MC simulations for the heparin fragments tested for their association with IFN-γ.

Rigid Bead Hydrodynamic Modeling of IFN-γ. We model the entire IFN-γ in solution as a rigid assembly of beads, with one large bead of radius a_1 (to represent the core structure) and a linear rigid chain of N_s beads of hydrodynamic radius a_2 (to represent the C-terminal tails), the total volume of the beads being constrained to represent hydrated IFN-γ, and the R_h to fit the experimental value of 3.0 nm. Note that a sphere with a 3 nm radius would fit the R_h requirement but not the volume one. Figure 6 shows the results for some models. The general organization of all models is similar with the largest dimension being 12.5 ± 1 nm and a transversal dimension being 5.7 ± 0.3 nm, while the ratio of the radii of the two types of beads can vary

N_s	a_1, nm	a_2, nm	L, nm
6	2.05	0.96	11.5
8	2.20	0.74	11.8
10	2.26	0.61	12.2
12	2.30	0.52	12.5
20	2.36	0.34	13.6

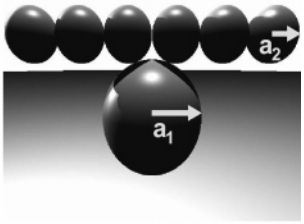

FIGURE 6: Rigid bead hydrodynamic modeling of IFN-γ. a_1 and a_2 are the radii of the large and small beads, respectively; N_s is the number of small beads, and L is the largest dimension (nanometers). The models are all compatible with the hydrated volume and experimental R_h value of IFN-γ.

FIGURE 7: Bead modeling of the heparin fragments.

extensively. The maximal extension of the whole IFN-γ with completely extended C-termini is 16 nm. It is longer than the arms in Figure 6, which is understandable because the C-termini in solution are probably flexible. The maximum ellipsoid dimensions of the IFN-γ core can be estimated as 4.5, 3.5, and 5.3 nm for the axes, corresponding to the volume of a sphere with a 2.2 nm radius, on the order of magnitude of the core beads of our models. In conclusion, this simple description gives for IFN-γ an appropriate description in terms of hydrodynamics and structure.

Rigid Bead Hydrodynamic Modeling of Complexes of Heparin Fragments and IFN-γ. Our strategy was to consider simple geometrical arrangements compatible with our experimental data. The complex is considered typically without changes in the shape of the partners. Only the arms of IFN-γ were able to be shifted. For heparin fragments, a rigid chain is defined in a plane and composed of beads with a 0.61 nm radius, with the numbers of beads defined by the contour length of the fragments. It was considered either as a linear rigid assembly or as a succession of linear segments of four beads corresponding to the persistence length, the angle between the beads being chosen in such a way that the ratio of the contour length and mean end-to-end distance fits with the values given by Pavlov et al. from the hydrodynamic characterization of heparin (28). Models are shown in Figure 7. Table 3 shows that the R_h values calculated by HYDRO for linear and "curved" bead assemblies differ only modestly ($\pm$0.1 nm) and are close to experimental values. For IFN-γ, we selected, among the models reproducing its hydrodynamic properties, that for which the smallest beads have the same radius as in heparin models (0.61 nm) (Figure 6). The small bead assembly represents the hydrodynamic properties of the C-terminal extensions of IFN-γ. The dimensions of the smallest fragment of heparin studied here, $Hep_{7.7}$ ($N = 11$), are comparable to the dimensions of these extensions ($N = 10$), while the dimensions of $Hep_{11.2}$ and $Hep_{14.1}$ are 1.5 and 2 times larger ($N = 16$ and $N = 20$), respectively. The positions of the beads of the extensions of IFN-γ in complexes were allowed to follow the curvature of the heparin fragments in most of the models of the complex.

Table 3: Hydrodynamic Properties of Heparin Fragments via Comparison of Bead Modeling and Experience[a]

		N	R_h (nm)	$s_{20,w}$ (S)	L (nm)	$\langle h^2\rangle^{1/2}$ (nm)	$L/\langle h^2\rangle^{1/2}$
$Hep_{7.7}$	linear	11	2.3	1.6	13.4		1.0
	segment	11	2.3	1.6	13.6	11.9	1.1
	exp.		2.1	1.7	14	11.5	1.2
$Hep_{11.2}$	linear	16	3.0	1.8	19.5		1.0
	segment	16	2.9	1.8	19.8	14.5	1.3
	exp.		2.6	2.0	20	14	1.4
$Hep_{14.1}$	linear	20	3.5	1.9	24.4		1.0
	segment	20	3.4	1.9	24.7	15.5	1.6
	exp.		3	2.2	25	15.5	1.6

[a] Models consist of rigid assemblies of N beads with a bead radius of 0.61 nm. The representation of the models for heparin composed with segments is shown in Figure 7.

Figure 8 shows different models designed for the example of the complex formed by one IFN-γ and two fragments of $Hep_{7.7}$. Table 4 presents the results in terms of hydrodynamic radii and sedimentation coefficients calculated with HYDRO.

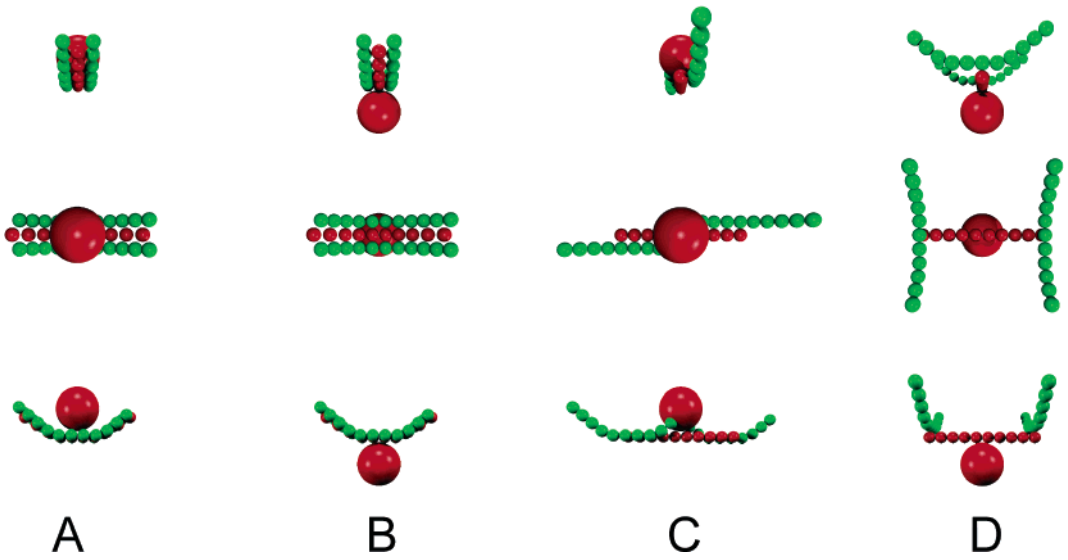

FIGURE 8: Bead models for the 2:1 $Hep_{7.7}$–IFN-γ complex. The models consist of nonoverlapping beads with radii of 0.61 and 2.26 nm. For each model, three orthogonal views are presented from top to bottom. Beads that represent IFN-γ are colored red; those representing heparin are colored green.

Table 4: Results of Hydrodynamic Bead Modeling of the 2:1 $Hep_{7.7}$−IFN-γ Complex[a]

model	R_h (nm)	$s_{20,w}$ (S)	model	R_h (nm)	$s_{20,w}$ (S)
A	3.40	4.40	C	4.08	3.68
B	3.68	4.08	D	4.77	3.15

[a] Models are presented in Figure 8. Experimental values for $s_{20,w}$, derived R_h, and R_h from size exclusion chromatography are 4.4 S, 3.4 nm, and 3.8 nm, respectively.

Model A is the most compact, with the two fragments of heparin parallel and constraining the IFN-γ arms and the protein core at the inside of the curvature. The modeled sedimentation coefficient has a value of 4.4 S found experimentally, as is the R_h of 3.4 nm inferred from $s_{20,w}$ and M_b. The value of R_h experimentally determined from size exclusion chromatography, 3.8 nm, differs slightly by 12%. We estimate the latter is the less precise one, and only the values of $s_{20,w}$ will be considered in the following for the comparison of the properties of the bead models with experience. Model B differs from model A in the position of the protein core in comparison to the heparin curvature. The calculated sedimentation coefficient for model B is ~10% smaller than that for model A (R_h is larger than for model A). Other more extended models, C and D, provide even smaller values for the sedimentation coefficients. Though there is not a unique geometry compatible with the experimental $s_{20,w}$ values, bead modeling suggests a rather compact complex.

Figure 9 presents a selected set of bead models for the different complexes of $Hep_{7.7}$, $Hep_{11.2}$, and $Hep_{14.1}$ with IFN-γ. The models were chosen to represent relatively compact structures. In all cases, the arms of IFN-γ are parallel to the fragment of heparin. In the case of the complex comprising a second fragment of heparin, the latter is positioned parallel to the former symmetrically in view of IFN-γ. For the longest $Hep_{14.1}$, the two molecules of IFN-γ are positioned in a head-to-tail manner. For all complexes, two configurations are presented, corresponding to the protein core(s) inside or outside the curvature of heparin. The selection was made because these simple arrangements model quite nicely the hydrodynamic properties of the various complexes. Most of the other arrangements would be less compact and lead to decreased $s_{20,w}$ values. The modeled sedimentation coefficients are given in Table 5. The values obtained for each complex in the two configurations differ by typically 10%. For the 1:1 $Hep_{7.7}$−IFN-γ and 1:2 $Hep_{14.1}$−IFN-γ complexes, best modeling of the $s_{20,w}$ values occurs with the slightly less compact configurations, with the protein core outside the curvature. For $Hep_{11.2}$ of intermediate size, the experimental values of $s_{20,w}$ are less precise, and the two models cannot be distinguished by their hydrodynamic properties. For the other complexes with which a second fragment of

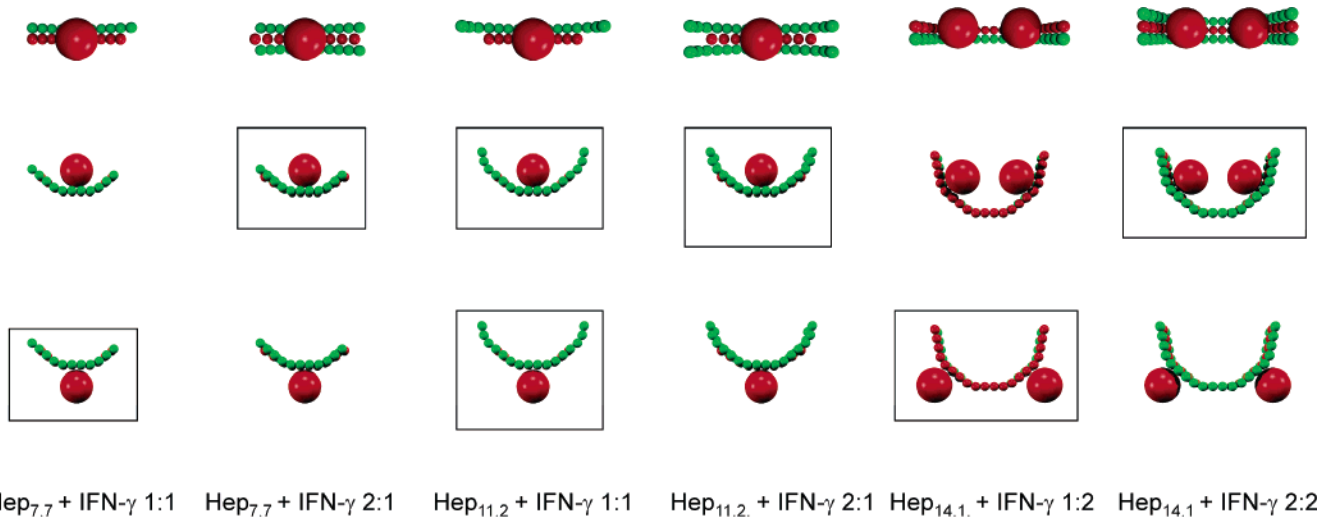

FIGURE 9: Bead models for complexes of IFN-γ with $Hep_{7.7}$, $Hep_{12.1}$, and $Hep_{14.1}$. For each complex, two models are presented: (top and middle) two orthogonal views of complexes with IFN-γ inside the curvature of the heparin fragment(s) and (bottom) complexes with IFN-γ outside the curvature of the heparin fragment(s). Beads that represent IFN-γ are colored red; those representing heparin are colored green. The rectangles denote models with hydrodynamic properties compatible with sedimentation velocity data.

Table 5: Hydrodynamic Modeling of $s_{20,w}$ Values for Complexes of IFN-γ with $Hep_{7.7}$, $Hep_{11.2}$, and $Hep_{14.1}$[a]

	calcd M ($\times 10^{-3}$ g/mol)	calcd $\bar{\nu}$ (mL/g)	exp. $s_{20,w}$ (S)	model	modeled $s_{20,w}$ (S)
1:1 $Hep_{7.7}$−IFN-γ	41.3	0.69	3.4 ± 0.1	IFN-γ inside	3.7
				IFN-γ outside	3.4
2:1 $Hep_{7.7}$−IFN-γ	49.0	0.65	4.4 ± 0.1	IFN-γ inside	4.4
				IFN-γ outside	4.1
1:1 $Hep_{11.2}$−IFN-γ	44.8	0.67	3.6 ± 0.3	IFN-γ inside	3.7
				IFN-γ outside	3.4
2:1 $Hep_{11.2}$−IFN-γ	56.0	0.63	4.9 ± 0.3	IFN-γ inside	4.6
				IFN-γ outside	4.2
1:2 $Hep_{14.1}$−IFN-γ	81.3	0.69	4.5 ± 0.2	IFN-γ inside	5.5
				IFN-γ outside	4.4
2:2 $Hep_{14.1}$−IFN-γ	95.4	0.66	6.1 ± 0.2	IFN-γ inside	6.1
				IFN-γ outside	5.4

[a] For each complex, hydrodynamic results for the two models presented in Figure 9 are given.

heparin is associated, the more compact configurations, with the core protein inside the curvature in Figure 9, lead to $s_{20,w}$ values closer to experimental ones.

DISCUSSION AND CONCLUSION

The study of HS and their complexes is made difficult because of their highly heterogeneous structure, the multiple possibilities of interactions, and the possible flexibility of the partners. We found here that analytical ultracentrifugation and size exclusion chromatography used in combination with hydrodynamic modeling are efficient tools for the description of the number of partners and their stoichiometry upon the interaction between proteic partners and HS or heparin fragments.

A Complex Pattern of Interactions of IFN-γ with Heparin. For each of the three heparin fragments studied here, two different types of complexes comprising one or two fragments of heparin are evidenced in the 10 μM range. Equilibrium between the species is clearly seen for the smallest fragment of heparin ($Hep_{7.7}$), with clear and logical concentration dependence for the two types of complexes. Because the different species are resolved in sedimentation velocity and size exclusion chromatography, the time scale of the equilibrium is rather large (longer than minutes). The concentration dependency was not investigated for IFN-γ−$Hep_{11.2}$ complexes. In the case of the mixtures of IFN-γ and $Hep_{14.1}$, the effects of the concentration of the partners are not obvious, and it is possible that the equilibrium conditions are not realized. Very slow kinetics could be related to multiple attachment possibilities of IFN-γ on this large fragment. Depending of the size of the heparin fragment, 1:1, 1:2, 2:1, and 2:2 IFN-γ−heparin complexes are described, in addition to aggregates. These aggregates were found with the large fragment of heparin, $Hep_{19.6}$, which comprises 34 disaccharides and has a contour length of 35 nm, more than twice the maximum possible extension of IFN-γ. They were found also when using IFN-γ that had been aged or frozen in solution.

Association Scheme in Relation to the Size of the Partners and Their Multiple Binding Possibilities. The different stoichiometries for the IFN-γ−heparin complexes were deduced from complementary sedimentation velocity and size exclusion chromatography experiments. The hydrodynamic radii were checked to be compatible with that calculated from hydrodynamic modeling for reasonable assemblies of the partners. Despite the diversity of the association states, the association schemes can be easily rationalized. The two smallest fragments of heparin, $Hep_{7.7}$, and $Hep_{11.2}$, have contour lengths of 14 and 20 nm, respectively. They were found to form two types of complex with IFN-γ. The smallest ones comprise one IFN-γ and one heparin fragment. The largest ones comprise two fragments of heparin. IFN-γ has binding sites on each of the C-terminal ends of the constituent monomers. These results show that the two binding sites on IFN-γ can separately recruit heparin. This can be related to the fact that either of the two binding sites on IFN-γ is free on the 1:1 complex or can exchange heparin. The longer fragment, $Hep_{14.1}$, has a contour length of 25 nm that exceeds significantly the maximum dimension of 16 nm for the protein in a completely extended conformation. From the two complexes evidenced in our experiments, the smallest one comprises two molecules of IFN-γ bound to the heparin fragment, and hydrodynamic bead modeling is compatible with their location along the long molecule. The larger complex comprises a second fragment of heparin corresponding to, at least, one of the four C-termini from the two IFN-γ dimers interacting with a second polysaccharide.

Compactness of the Shape of the Complexes. Hydrodynamic modeling was conducted not only to check the coherence in terms of the dimension of the proposed stoichiometries but also to investigate the compactness of the complex and eventual conformational changes of the partners. The hydrodynamic properties of rigid bead assemblies representing the complexes were calculated for simple geometries and compared to experiment. Good agreements between modeled and experimental values were found considering complexes without, or with only very slight, deformation of the individual partners. This suggests that complexation can be done without major conformational changes of the partners. It should not be forgotten, however, that there is in general not a single model corresponding to a modeled R_h. For example, we selected logically for heparin fragments the "curved" representation corresponding to their mean conformation inferred from heparin rigidity. However, because the persistence length of heparin (4.5 nm) compares with the contour length of the fragments investigated here, the R_h values of heparin represented in a linear or curved form do not differ significantly. Hydrodynamic modeling of the translational diffusion would require values of R_h much more precise than those experimentally obtained here for detection of other more than large conformational changes in heparin fragments or C-terminal ends of IFN-γ upon complex formation. Using neutron scattering would be in principle a powerful tool for obtaining low-resolution structure and particularly for describing the topologies and conformational change of the partners within the complex (*42*). Hydrodynamic studies such as those performed here give indications of the difficulties to be addressed in a scattering study, since the mixtures of heparin fragment with IFN-γ are rather fragile, composed of complexes that are in equilibrium and eventually of comparable size, i.e., hardly separable. Bead modeling of the complexes excludes extended models and clearly indicates rather compact structures. In particular, when two heparin fragments are bound, models corresponding to the two heparin fragments parallel and placed side by side reproduce the small values of experimental R_h. It suggests the two heparin molecules are in the proximity of each other and are not able to explore a large conformational space. Furthermore, bead modeling suggests more compact structures for complexes comprising two heparin fragments when compared to those comprising only one heparin fragment. This is represented by the core of IFN-γ situated in Figure 9 in the inside or outside part of the curvature of heparin fragment(s).

Unexpected Association States. Complex formation is observed in all heparin/IFN-γ mixtures investigated here, including those that are smaller than the minimum domain of interaction that was found for IFN-γ interacting with HS of human skin fibroblast [21−24 disaccharides (*27*)]. $Hep_{7.7}$ and $Hep_{11.2}$, which comprise 13 and 19 disaccharides, respectively, are found to bind IFN-γ, and the larger $Hep_{14.1}$, comprising 24 disaccharides, binds two molecules of IFN-γ. The fact that complex formation occurs for a smaller

fragment of heparin may be related to charge repartition. Heparin has a high charge content, and the charge is regularly distributed; the minimum fragment of HS that binds to heparin was found to comprise a central part of 15 to 16 disaccharides with low charge density (*27*). It is also worth noting that in the human skin fibroblast HS, from which the IFN-γ binding domain was isolated, the S-domains are separated from each other by a minimum of 15 poorly sulfated disaccharides. Presumably, using HS from other sources, such as liver HS in which the S-domains are linked by very short A-sequences (*43*), would have given rise to smaller binding domains. It was recently shown that synthetic molecules of limited length (11.5 nm) and composed two S-domains each of four disaccharides linked with a flexible neutral spacer (*44*) have high affinity for IFN-γ (*29*). Does HS flexibility allow larger conformational changes than heparin? One hypothesis would be that greater HS possible flexibility could be related to a lower charge density when compared to the highly charged heparin. However, the electrostatic contribution was found to be a minor part of the equilibrium rigidity of heparin, which is thus mainly determined by a structural contribution (*28*). It is thus expected that HS and heparin would not differ in their rigidity. We have measured some hydrodynamic properties of a fragment of HS from porcine intestinal mucosa (Celsus). Density, sedimentation velocity, and artificial boundary low-speed AUC experiments were performed under the same condition that was used for heparin fragments (*28*). Our measurements show indeed that the hydrodynamic behaviors of the HS fragment (9000 g/mol) and heparin fragment of same mass do not significantly differ in solution. Thus, the dimensions of HS and heparin, at least in this range of molecular mass, do not differ significantly. Of course, the study of this HS fragment does not exclude the possibility that other HS fragments are more flexible or can undergo conformational changes in relation to specific polysaccharide motifs. For example, the conformational lability of iduronic acid was thought to explain specific interaction capabilities of HS (*45*). Although this residue is rarely found in poorly sulfated regions, it is possible that in native HS, in which the two S-domains interacting with IFN-γ are separated by 15 or 16 disaccharides, such a flexibility could be important or even necessary for the formation of a 1:1 stoichiometric complex assembly. There are few data about the physical properties of the sequences that form the weakly sulfated regions of HS; however, it has been suggested that flexible linkage geometries may characterize these domains of the molecule, and bending of the *N*-acetyl rich regions has been proposed to explain how two spaced S-domains in HS can interact with different proteins (*46*). Our data suggested that HS and heparin have the same rigidity in solution, but it is possible that a bending of the internal domain is induced upon binding to the cytokine to meet the needs for proper binding geometry. In that case, the formation of the complex and the adoption of the proper orientation and spacing of the S-domains should be accompanied by an unfavorable loss of entropy. Whether such induced distortion is possible within the A-domain is probably unknown, but it is worth noting that the crystal structure of several heparin−protein complexes has revealed a marked distortion in the helical axis of the polymer (*9*). In the study presented here, IFN-γ−heparin complexes have dimensions compatible with binding without major conformational changes in the partners. However, we did not identify a 1:1 complex between IFN-γ and large heparin fragments.

In Vivo HS−IFN-γ Interaction. Finally, it is important to note that initial studies were all performed with isolated and soluble molecules, thus with conditions far from those found at the cell surface where HS are immobilized at high density. In such meshwork, a single protein can presumably interact simultaneously with several domains belonging to different chains. In this context, the unexpected numerous association states of IFN-γ and heparin evidenced here are most probably highly biologically relevant. The multiple possibilities of interaction of IFN-γ with relatively small charged fragments of HS relate logically to the possibility of local accumulation of the cytokine in tissues. The fact that more than one cytokine would interact with a long HS fragment and the fact that one cytokine can interact with two different polysaccharide chains suggest the possibilities of networks of interactions at the crowed surface of the cells. In particular, this study suggests that depending on the molecular organization of the HS chains (for example, the number and frequency of the S-domains along the chain) different complexes can be formed. It will be interesting to see whether such different complexes exist at the cell surface and have different biological activities. These interactions should be necessary for the concentration, protection, and storage of IFN-γ in tissues as well as for targeting it to its membrane receptor.

ACKNOWLEDGMENT

Jean Chang is acknowledged for his help in molecular modeling.

REFERENCES

1. Bernfield, M., Gotte, M., Park, P. W., Reizes, O., Fitzgerald, M. L., Lincecum, J., and Zako, M. (1999) Functions of cell surface heparan sulfate proteoglycans, *Annu. Rev. Biochem. 68*, 729−77.
2. Iozzo, R. V. (1998) Matrix proteoglycans: From molecular design to cellular function, *Annu. Rev. Biochem. 67*, 609−52.
3. Liu, J., and Thorp, S. C. (2002) Cell surface heparan sulfate and its roles in assisting viral infections, *Med. Res. Rev. 22*, 1−25.
4. Sasisekharan, R., Shriver, Z., Venkataraman, G., and Narayanasami, U. (2002) Roles of heparan-sulphate glycosaminoglycans in cancer, *Nat. Rev. Cancer 2*, 521−8.
5. Whitelock, J. M., and Iozzo, R. V. (2005) Heparan sulfate: A complex polymer charged with biological activity, *Chem. Rev. 105*, 2745−64.
6. Lindahl, U., Kusche-Gullberg, M., and Kjellen, L. (1998) Regulated diversity of heparan sulfate, *J. Biol. Chem. 273*, 24979−82.
7. Aaronson, D. S., and Horvath, C. M. (2002) A road map for those who don't know JAK-STAT, *Science 296*, 1653−5.
8. Murphy, K. J., Merry, C. L., Lyon, M., Thompson, J. E., Roberts, I. S., and Gallagher, J. T. (2004) A new model for the domain structure of heparan sulfate based on the novel specificity of K5 lyase, *J. Biol. Chem. 279*, 27239−45.
9. Mulloy, B., and Linhardt, R. J. (2001) Order out of complexity: Protein structures that interact with heparin, *Curr. Opin. Struct. Biol. 11*, 623−8.
10. Harmer, N. J., Ilag, L. L., Mulloy, B., Pellegrini, L., Robinson, C. V., and Blundell, T. L. (2004) Towards a resolution of the stoichiometry of the fibroblast growth factor (FGF)-FGF receptor-heparin complex, *J. Mol. Biol. 339*, 821−34.
11. Lortat-Jacob, H., Grosdidier, A., and Imberty, A. (2002) Structural diversity of heparan sulfate binding domains in chemokines, *Proc. Natl. Acad. Sci. U.S.A. 99*, 1229−34.
12. Boehm, U., Klamp, T., Groot, M., and Howard, J. C. (1997) Cellular responses to interferon-γ, *Annu. Rev. Immunol. 15*, 749−95.

13. Schroder, K., Hertzog, P. J., Ravasi, T., and Hume, D. A. (2004) Interferon-γ: An overview of signals, mechanisms and functions, *J. Leukocyte Biol. 75*, 163−89.
14. Billiau, A. (1996) Interferon-γ: Biology and role in pathogenesis, *Adv. Immunol. 62*, 61−130.
15. Ramana, C. V., Gil, M. P., Schreiber, R. D., and Stark, G. R. (2002) Stat1-dependent and -independent pathways in IFN-γ-dependent signaling, *Trends Immunol. 23*, 96−101.
16. Lortat-Jacob, H., Kleinman, H. K., and Grimaud, J. A. (1991) High-affinity binding of interferon-γ to a basement membrane complex (matrigel), *J. Clin. Invest. 87*, 878−83.
17. Lortat-Jacob, H., Brisson, C., Guerret, S., and Morel, G. (1996) Non-receptor-mediated tissue localization of human interferon-γ: Role of heparan sulfate/heparin-like molecules, *Cytokine 8*, 557−66.
18. Lortat-Jacob, H., Baltzer, F., and Grimaud, J. A. (1996) Heparin decreases the blood clearance of interferon-γ and increases its activity by limiting the processing of its carboxyl-terminal sequence, *J. Biol. Chem. 271*, 16139−43.
19. Lortat-Jacob, H., and Grimaud, J. A. (1991) Interferon-γ binds to heparan sulfate by a cluster of amino acids located in the C-terminal part of the molecule, *FEBS Lett. 280*, 152−4.
20. Ealick, S. E., Cook, W. J., Vijay-Kumar, S., Carson, M., Nagabhushan, T. L., Trotta, P. P., and Bugg, C. E. (1991) Three-dimensional structure of recombinant human interferon-γ, *Science 252*, 698−702.
21. Samudzi, C. T., and Rubin, J. R. (1993) Structure of recombinant bovine interferon-γ at 3.0 Å resolution, *Acta Crystallogr. D49*, 513−21.
22. Walter, M. R., Windsor, W. T., Nagabhushan, T. L., Lundell, D. J., Lunn, C. A., Zauodny, P. J., and Narula, S. K. (1995) Crystal structure of a complex between interferon-γ and its soluble high-affinity receptor, *Nature 376*, 230−5.
23. Randal, M., and Kossiakoff, A. A. (2000) The 2.0 Å structure of bovine interferon-γ: Assessment of the structural differences between species, *Acta Crystallogr. D56*, 14−24.
24. Vanhaverbeke, C., Simorre, J. P., Sabir, R., Gans, P., and Lortat-Jacob, H. (2004) NMR characterisation of the interaction between the C-terminal domain of interferon-γ and heparin-derived oligosaccharides, *Biochem. J. 384*, 93−9.
25. Sadir, R., Forest, E., and Lortat-Jacob, H. (1998) The heparan sulfate binding sequence of interferon-γ increased the on rate of the interferon-γ−interferon-γ receptor complex formation, *J. Biol. Chem. 273*, 10919−25.
26. Mulloy, B., Forster, M. J., Jones, C., and Davies, D. B. (1993) NMR. and molecular-modelling studies of the solution conformation of heparin, *Biochem. J. 293* (Part 3), 849−58.
27. Lortat-Jacob, H., Turnbull, J. E., and Grimaud, J. A. (1995) Molecular organization of the interferon γ-binding domain in heparan sulphate, *Biochem. J. 310* (Part 2), 497-505.
28. Pavlov, G., Finet, S., Tatarenko, K., Korneeva, E., and Ebel, C. (2003) Conformation of heparin studied with macromolecular hydrodynamic methods and X-ray scattering, *Eur. Biophys. J. 32*, 437−49.
29. Sarrazin, S., Bonnaffe, D., Lubineau, A., and Lortat-Jacob, H. (2005) Heparan Sulfate Mimicry: A synthetic glycoconjugate that recognizes the heparin binding domain of interferon-γ inhibits the cytokine activity, *J. Biol. Chem. 280*, 37558−64.
30. Haelewyn, J., and De Ley, M. (1995) A rapid single-step purification method for human interferon-γ from isolated *Escherichia coli* inclusion bodies, *Biochem. Mol. Biol. Int. 37*, 1163−71.
31. Berg, K., Hansen, M. B., and Nielsen, S. E. (1990) A new sensitive bioassay for precise quantification of interferon activity as measured via the mitochondrial dehydrogenase function in cells (MTT-method), *APMIS 98*, 156−62.
32. Clark, M., Cramer, R. D. I., and van den Opdenbosch, N. (1989) Validation of the general purpose Tripos 5.2 force field, *J. Comput. Chem. 10*, 982−1012.
33. Imberty, A., Bettler, E., Karababa, M., Mazeau, K., Petrova, P., and Pérez, S. (1999) Building sugars: The sweet part of structural biology, in *Perspectives in Structural Biology* (Vijayan, M., Yathindra, N., and Kolaskar, A. S., Eds.) pp 392−409, Indian Academy of Sciences and Universities Press, Hyderabad, India.
34. Waldherr-Teschner, M., Goetze, T., Heiden, W., Knoblauch, M., Vollhardt, H., and Brickmann, J. (1992) MOLCAD: Computer Aided Visualization and Manipulation of Models in Molecular Science, in *Advances in Scientific Visualization* (Post, F. H., and Hin, A. J. S., Eds.) pp 58−67, Springer, Heidelberg, Germany.
35. Dam, J., and Schuck, P. (2004) Calculating Sedimentation Coefficient Distributions by Direct Modeling of Sedimentation Velocity Concentration Profiles, *Methods Enzymol. 384*, 185−212.
36. Schuck, P. (2000) Size-distribution analysis of macromolecules by sedimentation velocity ultracentrifugation and lamm equation modeling, *Biophys. J. 78*, 1606−19.
37. García de la Torre, J., Navarro, S., Lopez Martinez, M. C., Diaz, F. G., and Lopez Cascales, J. J. (1994) HYDRO: A computer program for the prediction of hydrodynamic properties of macromolecules, *Biophys. J. 67*, 530−1.
38. Schellman, J. A. (1974) Flexibility of DNA, *Biopolymers 13*, 217−26.
39. Hagerman, P., and Zimm, B. (1981) Monte Carlo approach to the analysis of the rotational diffusion of wormlike chains, *Biopolymers 20*, 1481−502.
40. Garcia de la Torre, J., Perez Sanchez, H. E., Ortega, A., Hernandez, J. G., Fernandes, M. X., Diaz, F. G., and Lopez Martinez, M. C. (2003) Calculation of the solution properties of flexible macromolecules: Methods and applications, *Eur. Biophys. J. 32*, 477−86.
41. Iniesta, A., and García de la Torre, J. (1990) A second-order algorithm for the simulation of the Brownian dynamics of macromolecular models, *J. Chem. Phys. 92*, 2015−9.
42. Koch, M. H., Vachette, P., and Svergun, D. I. (2003) Small-angle scattering: A view on the properties, structures and structural changes of biological macromolecules in solution, *Q. Rev. Biophys. 36*, 147−227.
43. Lyon, M., Deakin, J. A., and Gallagher, J. T. (1994) Liver heparan sulfate structure. A novel molecular design, *J. Biol. Chem. 269*, 11208−15.
44. Lubineau, A., Lortat-Jacob, H., Gavard, O., Sarrazin, S., and Bonnaffe, D. (2004) Synthesis of tailor-made glycoconjugate mimetics of heparan sulfate that bind IFN-γ in the nanomolar range, *Chemistry 10*, 4265−82.
45. Casu, B., Petitou, M., Provasoli, M., and Sinay, P. (1988) Conformational flexibility: A new concept for explaining binding and biological properties of iduronic acid-containing glycosaminoglycans, *Trends Biochem. Sci. 13*, 221−5.
46. Mulloy, B., and Forster, M. J. (2000) Conformation and dynamics of heparin and heparan sulfate, *Glycobiology 10*, 1147−56.
47. Metropolis, N., Metropolis, A., Rosenbluth, M., Teller, A., and Teller, E. (1953) Equation of state calculation by fast computing machines, *J. Chem. Phys. 21*, 1087−1093.

BI061490W